AIAA 82-4297

Hyperballistic Vehicle Dynamics

Lars E. Ericsson*
Lockheed Missiles & Space Company, Inc., Sunnyvale, California

An earlier developed embedded Newtonian theory for prediction of the unsteady aerodynamics of hemisphere-cylinder-flare bodies has been extended to other hyperballistic geometries of general interest. Using generalized embedded Newtonian theory, the effect of Mach number is accounted for down to moderate supersonic speeds. The nose geometry can be described analytically or given in tabular form for a slender axisymmetric shape, which can include slope discontinuities. The "embedded" aft body can also be of a general shape, described by a series of conical segments, including the cylinder as a conical segment of zero slope.

Nomenclature

A = axial force coefficient, $C_A = A/(\rho_\infty U_\infty^2/2)S$
A_1, A_2 = constants, Eq. (10)
ΔA = surface area element (Fig. 1)
C_γ = parameter defined in Eq. (22)
c = reference length, usually $c = d_N$
d = diameter of cylindric aft body
d_N = base diameter of nosetip
D_N = nose drag coefficient, $C_{DN} = D_N/(\rho_\infty U_\infty^2/2)(\pi d_N^2/4)$
f^*, f_a^* = dynamic pressure ratio, $= \rho U^2/\rho_\infty U_\infty^2$
f_0^* = minimum value of f^*
g^* = velocity ratio, $= U/U_\infty$
g_0^* = minimum value of g^*
K_N = hypersonic similarity parameter, $= M_\infty \sin\theta_N$
K^* = shock parameter defined in Eqs. (5) and (6)
l_N, L_N = nose length
L_N^* = nose length parameter defined by Eq. (49) and Fig. 3
M = Mach number
M_p = pitching moment, coefficient $C_m = M_p/(\rho_\infty U_\infty^2/2)Sc$
$M^*, M^{**}, \bar{M}^*$ = Mach numbers defined by Eqs. (23-25)
N = normal force, coefficient $C_N = N/(\rho_\infty U_\infty^2/2)S$
p = static pressure, coefficient $Cp = (p - p_\infty)/(\rho_\infty U_\infty^2/2)$
p_0 = blast wave pressure, coefficient $Cp_0 = (p_0 - p_\infty)/(\rho_\infty U_\infty^2/2)$, defined in Eq. (15)
q = rigid body pitch rate
r = body cross-sectional radius
r^* = nose geometry parameter defined by Eq. (49)
R = radial distance defined in Fig. 1
R_m = body radius defined in Fig. 2
Re = Reynolds number, $Re_d = U_\infty d/\nu_\infty$
R_{sh} = shock radius (Fig. 1)
S = reference area, $= \pi c^2/4$
t = time
U = axial velocity component
$\bar{U}$ = mean convection velocity
$V_\perp$ = velocity component normal to body surface
x = axial distance from nose shoulder (Fig. 1)
z = translatory coordinate (Fig. 1)
α = angle of attack
α_0 = trim angle of attack
α^*, α_{ST}^* = α values defined in Eq. (48) and Fig. 3
γ = ratio of specific heats, = 1.4 for air
Δ = increment and shock detachment distance (Fig. 2)
θ = body perturbation in pitch
θ_E = body surface slope (Fig. 1)
θ_m = maximum cone angle for attached shock (Fig. 2)
θ_n = nose surface slope
θ_N = nose cone half-angle
$\bar{\theta}_N$ = effective θ_N value defined by Eq. (13)
ν = kinematic viscosity of air
ξ = dimensionless x coordinate, $= x/c$
ρ = density of air
σ_{sh} = conic shock angle
τ^* = effective flow inclination, Eq. (48) and Fig. 3
ϕ = azimuth location (see Fig. 1)
ϕ_1 = Newtonian shadow definition, Eq. (60)
χ^* = hypersonic similarity parameter defined by Eq. (10)
ω = pitch frequency

Subscripts

a = attached bow shock
B = base and body
cg = center of gravity or moment reference center
E, ϵ = embedded
inst = instantaneous value
L = local value
max = maximum or stagnation value
N, n = nose
Newt = Newtonian value
sh = shock
$1,2$ = numbering subscript
∞ = freestream conditions

Superscripts

i = induced, e.g., Δ_{Cp}^i = nose-bluntness-induced pressure change on embedded aft body element
$(\bar{\ })$ = effective integrated mean value, e.g., $\bar{\theta}_N$, Eq. (13)

Derivative Symbols

$\dot{\alpha}$ = $\partial\alpha/\partial T, C_{N\dot{\alpha}} = \partial C_N/\partial\dot{\alpha}$
C_{mq} = $\partial C_m/\partial(cq/U_\infty)$: $C_{m\dot{\alpha}} = \partial C_m/\partial(c\dot{\alpha}/U_\infty)$
$C_{m\dot{\theta}}$ = $C_{mq} + C_{m\dot{\alpha}}$

Received Jan. 14, 1981; revision received March 23, 1982.

*Senior Consulting Engineer. Associate Fellow AIAA.

Introduction

AT hypersonic speeds, a blunt nose is often needed for thermodynamic survival. The nose-bluntness-induced curved bow shock generates a highly nonuniform flowfield, the "entropy wake," in which the aft body is embedded. The associated nonlinear unsteady aerodynamics were derived in Ref. 1. In the present paper, the theory of Ref. 1 is extended to more general geometries than the hemisphere-cylinder-flare body, and the effect of Mach number is accounted for down to moderate supersonic speeds where it can be joined with the theory of Ref. 2, thus providing the capability to compute the unsteady aerodynamic characteristics from $M=0$ to $M=\infty$.

Analysis

The embedded Newtonian theory developed earlier for prediction of the hypersonic unsteady aerodynamics of a hemisphere-cylinder-flare-body[1] will be modified to account for Mach number effects in a manner similar to what has been done earlier for slender blunted cones.[3] The method will also be extended to nose geometries of more practical interest than the pure hemisphere geometry, following an approach similar to the one used for slender cones.[4,5]

In the embedded Newtonian theory,[1] Newtonian concepts are used in the nonuniform inviscid flowfield defined by the bow shock.[6-8] The shock shape is defined by the nose bluntness and can be related to the nose drag.[9] The pressure coefficient on the "embedded" body element A in Fig. 1 can be written

$$Cp_E = Cp_0 + Cp_{\max}\left(\frac{V_\perp}{U}\right)^2 \frac{\rho U^2}{\rho_\infty U_\infty^2} \tag{1}$$

where $V_\perp$ is the local velocity component normal to the body surface and U is the axial velocity component; that is, $V_\perp/U$ is defined geometrically. For the body element ΔA in Fig. 1, pitching with the rate q rad/s, it is

$$\frac{V_\perp}{U} = \cos\alpha\,\sin\theta + \sin\alpha\,\cos\theta_E \sin\phi + \frac{(x-x_{cg}+r\tan\theta_E)\,q}{U}\cos\theta_E\sin\phi \tag{2}$$

On the embedded surface element $Cp_{\max}$ is given by the stagnation pressure behind a normal shock, which for Mach numbers of "Newtonian" interest, $M>2$, can be approximated as follows.[10]†

$$Cp_{\max} = \frac{\gamma+3}{\gamma+1}\left[1-\frac{1.5}{\gamma+3}\frac{1}{M^2}\right] \tag{3}$$

The dynamic pressure ratio is a function of radial position, and, assuming similar profiles, can be written as follows‡:

$$\frac{\rho U^2}{\rho_\infty U_\infty^2} = f^*\left(\frac{R}{R_{sh}}\right) \tag{4}$$

R_{sh} is determined by the nose drag

$$\frac{R_{sh}}{d_N} = K^* C_{DN}^{1/4}\left(\frac{x-x_{sh}}{d_N}\right)^{1/2} \tag{5}$$

†The data are correlated better with the numerator 1.5 rather than 2 in the Mach number term.

‡This is a good assumption, except for the flow region close to the bow shock, e.g., the near-nose region. Reference 11 shows the requirement to be $x/d_N \geq 2$ for $M \geq 10$, or $(x/d_N)/M^2\sqrt{C_D} \leq 0.1$

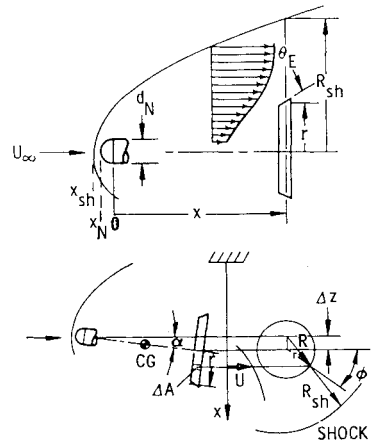

Fig. 1 Definition of embedded flow geometry.

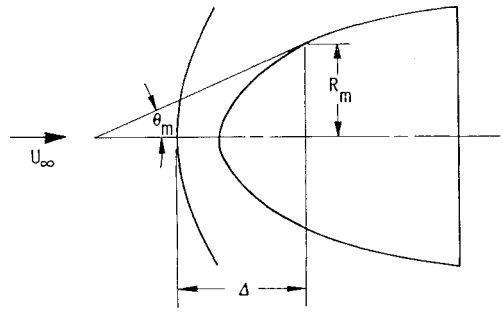

Fig. 2 Shock detachment distance for a general nose shape.[14]

In the hypersonic limit, K^* is a true constant. Comparing this first approximation with methods of characteristics (MOC) results[12] for a hemisphere-cylinder in air ($\gamma=1.4$), as is done in Ref. 11, gives $K^*=1.0$ with $Cp_{\max}$ defined by Eq. (3). This K^* value also correlates the experimental data in Ref. 9. Several suggestions for means to account for the Mach number effect have been made. Combining the one in Ref. 13 with the above hypersonic K^* value gives§

$$K^* = 1 + \frac{1.57}{M_\infty^2\sqrt{C_{DN}}}\frac{x-x_N}{d_N} - \frac{5.80}{M_\infty^4 C_{DN}}\left(\frac{x-x_N}{d_N}\right)^2 \tag{6}$$

For most applications of the embedded Newtonian concepts, the last term in Eq. (6) can be neglected and x_N can be substituted by x_{sh}.

Sinnot has devised simple means for determining the shock detachment distance from nosetips of rather general shape.[14,15] He uses the tangent cone of maximum cone half-angle allowing an attached shock, θ_m, to define a shock detachment distance Δ, as shown in Fig. 2; that is

$$\Delta/R_m = 0.77\cot\theta_m \tag{7}$$

For axisymmetric bodies, x_{sh} is determined by Eq. (7) and the nose geometry.

A closed-form expression for computation of the maximum cone angle θ_m for an attached shock on cones has been provided by Shanbag.[16]

$$\theta_m = \sin^{-1}\left\{\frac{1}{\gamma}\left[1-\frac{1.668}{M_\infty^2}-\frac{1.803}{M_\infty^4}+\frac{13.59}{M_\infty^6}\right]^{1/2}\right\} \tag{8}$$

§Reference 13 also gives the γ dependence.

Equations (5-8) define R_{sh} in Eq. (4). The parameter R needed in Eq. (4) is defined by Fig. 1 as follows:

$$\left(\frac{R}{d_N}\right)^2=\left(\frac{\Delta z}{d_N}\right)^2+2\frac{\Delta z}{d_N}\left(\frac{r}{d_N}\right)\cos\alpha\sin\phi$$
$$+\left(\frac{r}{d_N}\right)^2\{\cos^2\alpha\sin^2\phi+\cos^2\phi\}$$
$$\frac{\Delta z}{d_N}=\frac{x}{d_N}\sin\alpha+\left(\frac{\Delta z}{d_N}\right)\text{elastic} \tag{9}$$

The function $f^*(R/R_{sh})$ in Eq. (4) is of parabolic shape and can be written

$$f^*(R/R_{sh})=f_0^*+A_1\chi^*+A_2\chi^{*2}$$
$$\chi^*=\left(\frac{R}{d_N}-\frac{1}{2}\right)^2\Big/\left(\frac{R_{sh}}{d_N}\right)^2 \tag{10}$$

When the conic nosetip has an attached shock, $\theta_N<\theta_m$, f^* is the dynamic pressure ratio through a conic shock. If one assumes isentropic expansion over the cone-cylinder shoulder, the following value is obtained far downstream of the nose, where freestream static pressure is reached on the cylinder.[17,18]

$$f_a^*=\frac{\gamma+1}{\gamma-1}\frac{[(\gamma-1)M_\infty^2+2]\sin^2\sigma_{sh}}{[(\gamma-1)M_\infty^2\sin^2\sigma_{sh}+2]}$$
$$\times\left[\frac{\gamma+1}{2\gamma M_\infty^2\sin^2\sigma_{sh}-(\gamma-1)}\right]^{1/\gamma}-\frac{2}{(\gamma-1)M_\infty^2} \tag{11}$$

Using compressible flow cone tables,[17] f_a^* has been computed[18] as a function of the hypersonic similarity parameter for the nose cone, $K_N=M_\infty\sin\theta_N$. The following analytic approximation is obtained using Eq. (11) for $K_N\le 5$, and the detached shock limit for $K_N\to\infty$.

$$f_a^*=\begin{cases}1.0 & : K_N\le 1.25\\ 10^{-\left(\frac{K_N-1.25}{9.75}\right)} & : 1.25<K_N\le 11\\ 0.17 & : K_N>11\end{cases} \tag{12}$$

Holt's suggestion[18] to represent a pointed ogival nose with a cone of the same L_N/d_N ratio will not be followed. A more general approach is to find the cone that has the same forebody axial force as the nonconic nose shape. The entropy increase through the shock wave is proportional to the nose drag. Using the present modified Newtonian flow concepts, the nose drag for a ϕ-slice of a cone is

$$C_{DN}=C_\gamma C_{p\max}\sin^2\theta_N$$

Thus the equivalent nose cone angle in the ϕ-slice is

$$\bar\theta_N=\sin^{-1}\sqrt{C_{DN}/C_\gamma C_{p\max}} \tag{13}$$

When $\theta_N\le\theta_m$, the effective conic bow shock is attached and the embedded flow over the aft body will be uniform with a const dynamic pressure deficit for $\phi=$ const, determined by Eq. (12). When $\theta_N\not\le i_m$, the entropy wake is nonuniform with the dynamic pressure deficit given by Eq. (10) or its equivalent.

Blunt-Nose Cylinder Flare Bodies

Seiff's data for hemisphere-cylinder at high hypersonic speed[11-14] defines a dynamic pressure that can be fitted by the following polynomial

$$\rho U^2/\rho_\infty U_\infty^2=f^*(\chi^*)=0.17+2.75\chi^*+4\chi^{*2} \tag{14}$$

The blast wave pressure is constant over the radial extent of a submerged flare.[7,19] The pressure coefficient Cp_0 in Eq. (1) is, therefore, assumed to be constant. Kuehn[20] gives a correlation formula for the axial distribution of the blast wave pressure $p_0(0)$ on the blast wave centerline (also measured on the surface of a hemisphere cylinder).

This correlation is in excellent agreement with that obtained by Van Hise[12] for his MOC calculations. As before, x_{sh}/d_N will be substituted for x_N/d_N. This will improve the correlation somewhaht according to the experimental data in Ref. 21.

The following embedded Newtonian formulation is obtained for the aerodynamic pressure coefficient Cp_E on a surface embedded in the entropy wake generated by a blunt nose at high supersonic and hypersonic speeds ($\gamma=1.4$).

$$Cp_E=Cp_0+Cp_{\text{Newt}}f^*(\chi^*)$$
$$Cp_0=\frac{0.081C_{DN}^{1/2}}{\frac{x}{d_N}-\frac{x_{sh}}{d_N}}-\frac{0.64}{M_\infty^2} \tag{15}$$
$$Cp_{\text{Newt}}=Cp_{\max}\left(\frac{V_\perp}{U}\right)^2$$

The embedded axisymmetric body of general shape is represented by a series of conic frustums, which reduce to single- or multisegmented cylinder-flare bodies as special cases.

As presently developed, the complete information needed to apply Eq. (15) to the blunt-nosed cylinder-flare body exists only for $M_\infty\to\infty$. One needs to include the effects of finite Mach number in the dynamic pressure function $f^*(\chi^*)$, Eq. (14). It is shown in Ref. 3 how this Mach number effect for slender-blunted cones can be included by use of curve-fitted MOC results. The equation corresponding to Eq. (14) for the slender, spherically blunted cone is

$$f^*(\chi^*)=\begin{cases}0.17+1.375\chi^* & : \chi^*\le 0.49\\ 1-3.43\,(0.7-\chi^*)^2 & : 0.49<\chi^*<0.7\\ 1 & :\chi^*\ge 0.7\end{cases} \tag{16}$$

Comparing Eqs. (14) and (16), one feels compelled to investigate the effect of the last term in Eq. (14), i.e., $4\chi^{*2}$. Allowing no overshoot of the dynamic pressure, i.e., $\rho U^2\le\rho_\infty U_\infty^2$, one finds that $f^*=1$ for $\chi^*=0.245$ or $=0.302$ depending on whether or not one includes $4\chi^{*2}$ in the expression for f^*. Recognizing the fact that bow shock-flare shock interactions[22] will come into play when f^* exceeds unity, carrying the term $4\chi^{*2}$ may not provide improved accuracy. Consequently, f^* will be represented by a linear function of χ^* also for the flared body.

Using the linear approximation in χ^*, Eqs. (14) and (16) combine to the following formulation (for $M_\infty\to\infty$).

$$f^*(\chi^*)=0.17+\begin{cases}1.375\chi^*: \chi^*\le 0.604: \text{cone}\\ 2.750\chi^*: \chi^*\le 0.302: \text{cylinder}\end{cases} \tag{17}$$

In Ref. 3 no Mach number effect was considered in the definition of χ^*, i.e., $K^*=1$ in Eq. (5) and $Cp_{\max}=1.8$ for determination of C_{DN}. Instead, the coefficients for χ^*, as well

as the zero offset f_0^*, were made functions of Mach number to fit the MOC values. For the cylinder-flare body discussed here, it is, however, attractive to include the Mach number dependence in χ^* itself. Equations (3-6), (9), and (10) define the Mach number effects on χ^*. What is needed in addition is a formulation of how f_0^* varies with Mach number from the hypersonic value $f_0^* = 0.17$ to the near-unit value at low supersonic speeds.

Equation (17) indicates that one should be able to use the $f_0^*(M_\infty)$ function of Ref. 3. Thus,

$$\begin{aligned} f_0^* &= 0.17 + \left(\frac{9.65}{M_\infty + 8.7}\right)^3 && : M_\infty \geq 1.6 \\ &= 1.00: && : M_\infty < 1.6 \end{aligned} \tag{18}$$

The hypersonic velocity ratio $g^* = U/U_\infty$ given by Seiff's data[6] is

$$g^* = 0.67 + 0.60\chi^{*\,1/2} \tag{19}$$

Using the approach of Ref. 23 to determine the $g_0^*(M_\infty)$ function gives

$$g^* = 1 - 0.362\sqrt{1 - f_0^*} + 0.60\chi^{*\,1/2} \tag{20}$$

The embedded Mach number needed in Eq. (3) is for isentropic flow

$$M = M_\infty (g^*)^{\gamma+2} / (f^*)^{(\gamma-1)/2} \tag{21}$$

It was shown in Ref. 24 that the Mach number dependence of Cp_{Newt} in Eq. (15) can be obtained as follows using tangent cone methods and MOC results for $\alpha = 0$.

$$\begin{aligned} Cp_{TC} &= C_\gamma Cp_{\text{Newt}} \\ C_\gamma &= 1.01 + 1.31[\ln(10M\sin\theta)]^{-7/3} && : M\sin\theta \geq 0.4 \\ &= 1.625 && : M\sin\theta < 0.4 \end{aligned} \tag{22}$$

Cp_{Newt} in Eq. (15) is substituted by Cp_{TC} defined by Eq. (22). In Ref. 24, the lowest Mach number, $M_\infty = M_\infty^*$, for which the embedded Newtonian flow concepts could be used, was defined as $M_\infty^* = 0.4\text{cosec}\theta_c$, where θ_c is the half-angle for the conic frustum. Applying the same rule to the present geometry gives

$$M_\infty^* = 0.4\left[1 + \left(\frac{2(x_B/d_N)}{(d_B/d_N) - 1}\right)^2\right]^{1/2} \tag{23}$$

This gives a very conservative value, and the embedded Newtonian characteristics are going to provide a good approximation for Mach numbers below the value given by Eq. (23). On the other hand, an unconservative value, down to which the embedded Newtonian characteristics will not provide a good approximation, is given by

$$M_\infty^{**} = 0.4\left[1 + 4\left(\frac{(x_B/d_N) + (L_N/d_N)}{(d_B/d_N)}\right)^2\right]^{1/2} \tag{24}$$

For simplicity, the lower boundary for the embedded Newtonian method will be represented by

$$\overline{M}_\infty^* = (M_\infty^* + M_\infty^{**})/2 \tag{25}$$

Differentiating Eq. (15), as modified by Eq. (22), with respect to angle of attack gives

$$(Cp_\alpha)_E = (Cp_{\alpha L})_1 + (Cp_{\alpha L})_2 + (\Delta^i Cp_\alpha)_1 + (\Delta^i Cp_\alpha)_2 \tag{26a}$$

$$(Cp_{\alpha L})_1 = C_\gamma \frac{\partial Cp_{\text{Newt}}}{\partial\alpha} f^* \tag{26b}$$

$$(Cp_{\alpha L})_2 = \frac{\partial Cp_0}{\partial C_{DN}} \frac{dC_{DN}}{d\alpha} \tag{26c}$$

$$(\Delta^i Cp_\alpha)_1 = C_\gamma Cp_{\text{Newt}} \frac{\partial f^*}{\partial(\Delta z/d_N)} \frac{d(\Delta z/d_N)}{d\alpha} \tag{26d}$$

$$(\Delta^i Cp_\alpha)_2 = C_\gamma Cp_{\text{Newt}} \frac{\partial f^*}{\partial C_{DN}} \frac{dC_{DN}}{d\alpha} \tag{26e}$$

where $(Cp_{\alpha L})_1$ is the local pressure change caused by (unit) attitude change; $(Cp_{\alpha L})_2$ is the change in blast wave pressure (Cp_0) due to unit attitude effect on nose drag; $(\Delta^i Cp_\alpha)_1$ is the pressure change on the embedded surface element caused by the relative translatory deflection between nosetip and body element through (unit) attitude change (α); and $(\Delta^i Cp_\alpha)_2$ is the pressure change on the embedded surface element caused by the nose drag change through (unit) change of nosetip attitude.

From Eqs. (2), (15), (22), and (26), one obtains

$$(Cp_{\alpha L})_1 = C_\gamma C_{p\alpha\text{Newt}} f^* \tag{27a}$$

$$\begin{aligned} Cp_{\alpha\text{new}t} &= 2Cp_{\max}(\cos\alpha\sin\theta_c + \sin\alpha\cos\theta_c\sin\phi) \\ &\times(\cos\alpha\cos\theta_c\sin\phi - \sin\alpha\sin\theta_c) \end{aligned} \tag{27b}$$

$$(Cp_{\alpha L})_2 = \frac{\partial Cp_0}{\partial C_{DN}} C_{DN\alpha} \tag{28a}$$

$$\begin{aligned} \frac{\partial Cp_0}{\partial C_{DN}} &= 0 && : \bar{\theta}_N \leq \theta_m \\ &= \frac{k_\gamma}{2C_{DN}^{1/2}(x/d_N - x_{sh}/d_N)} && : \bar{\theta}_N > \theta_m \end{aligned} \tag{28b}$$

where $k_\gamma = 0.098\ (\gamma - 1)^{0.395} = 0.067$ for $\gamma = 1.4$

$$(\Delta^i Cp_\alpha)_1 = C_\gamma Cp_{\text{Newt}} \frac{\partial f^*}{\partial(\Delta z/d_N)} \frac{d(\Delta z/d_N)}{d\alpha} \tag{29a}$$

$$\begin{aligned} \frac{\partial f^*}{\partial\left(\frac{\partial z}{d_N}\right)} &= \theta && : \bar{\theta}_N \leq \theta_m \\ &= 2\chi^* \frac{\partial f^*}{\partial\chi^*} \frac{\frac{\Delta z}{d_N} + \frac{r}{d_N}\cos\alpha\sin\theta_c}{\frac{R}{d_N}\left(\frac{R}{d_N} - \frac{1}{2}\right)} && : \bar{\theta}_N > \theta_m \end{aligned} \tag{29b}$$

$d(\delta z/d_N)/d\alpha$, from Eq. (9), is $d(\delta/d_N)/d\alpha = x/d_N \cos\alpha$ for a rigid body

$$(\Delta^i Cp_\alpha)_2 = C_\gamma Cp_{\text{Newt}} \frac{\partial f^*}{\partial C_{DN}} C_{DN\alpha}$$

$$\bar{\theta}_N < \theta_m: \frac{\partial f^*}{\partial C_{DN}} = 0 \qquad : K_N \le 1.25$$

$$= -\frac{0.118 K_N}{C_{DN}} f_a^* \qquad : 1.25 < K_N < 11$$

$$= 0 \qquad : K_N \ge 11$$

$$\bar{\theta}_N > \theta_m: \frac{\partial f^*}{\partial C_{DN}} = -\frac{\chi^*}{2K^* C_{DN}} \frac{\partial f^*}{\partial \chi^*} \left[1 - 1.57 \left(\frac{\frac{x - x_{sh}}{d_N}}{M_\infty^2 C_{DN}^{1/2}} \right) + 17.4 \left(\frac{\frac{x - x_{sh}}{d_N}}{M_\infty^2 C_{DN}^{1/2}} \right)^2 \right] \tag{30}$$

Unsteady Aerodynamics

The unsteady aerodynamic characteristics are determined as follows. The effect of pitch rate q is obtained by considering that

$$\partial/\partial\left(\frac{cq}{U_\infty}\right) = \frac{1}{g^*} \partial/\partial\left(\frac{cq}{U}\right) \tag{31}$$

The effect of time lag on the relative translatory position of the body element in the inviscid shear flow is

$$\Delta z = z(x,t) - z(0, t - \Delta t) \tag{32}$$

A time lag Δt occurs before a translation of the blast wave generator, the nose, has resulted in a translation of the shear flow at the body element. This time lag is

$$\Delta t = (x\cos\alpha - r\sin\alpha\sin\theta_\epsilon)/g^* U_\infty \tag{33}$$

For slow oscillations, $(cq/U_\infty)^2 \ll 1$, Δz can be written

$$\Delta z = \Delta z_{\text{inst}} + \Delta z(\Delta t)$$

$$\Delta z_{\text{inst}} = z(x,t) - z(0,t) \tag{34}$$

$$\Delta z(\Delta t) = \Delta t \dot{z}(0,t)$$

With Eq. (33), $\Delta z\ (\Delta t)$ becomes

$$\Delta z(\Delta t) = \frac{\dot{z}(0,t)}{g^* U_\infty} (x\cos\alpha - r\sin\alpha\sin\theta_\epsilon) \tag{35}$$

For a rigid vehicle describing oscillations in pitch around cg (Fig. 1), one obtains the following definition of z

$$\frac{z}{d_N} = \frac{z_{cg}}{d_N} + \left(\frac{x}{d_N} - \frac{x_{cg}}{d_N}\right)\sin\alpha \tag{36}$$

Thus,

$$\frac{\dot{z}}{d_N} = \frac{\dot{z}_{cg}}{d_N} + \left(\frac{x}{d_N} - \frac{x_{cg}}{d_N}\right)(\cos\alpha)\,\dot{\alpha} \tag{37}$$

where $\dot{\alpha} = q$.

The convective time lag before the effect of a change of nose drag is felt by the submerged body element is also Δt, as defined by Eq. (33).

Differentiating Eq. (15) with respect to (cq/U), utilizing Eqs. (10), (26), and (31), gives the following local dynamic derivatives due to pitch rate.

$$(Cp_q)_1 = \frac{\partial Cp_E}{\partial\left(\frac{V_\perp}{U}\right)} \frac{\partial\left(\frac{V_\perp}{U}\right)}{\partial\left(\frac{cq}{U_\infty}\right)} = C_\gamma Cp_{q\text{Newt}} f^*/g^* \tag{38a}$$

$$Cp_{q\text{Newt}} = 2Cp_{\max}\left(\frac{d_N}{c}\right)\left(\frac{x}{d_N} - \frac{x_{cg}}{d_N} + \frac{r}{d_N}\tan\theta_\epsilon\right) \times (\cos\alpha\sin\theta_\epsilon + \sin\alpha\cos\theta_\epsilon\sin\phi)\cos\theta_\epsilon\sin\phi \tag{38b}$$

$$(Cp_q)_2 = \frac{\partial Cp_0}{\partial C_{DN}} \frac{\partial C_{DN}}{\partial\left(\frac{V_\perp}{U}\right)} \frac{d\left(\frac{V_\perp}{U}\right)_N}{d\left(\frac{cq}{U_\infty}\right)} \tag{39a}$$

$$\frac{\partial Cp_0}{\partial C_{DN}} = 0 \qquad : \bar{\theta}_N \le \theta_m$$

$$= \frac{k_\gamma}{\left|2C_{DN}^{1/2}\left(\frac{x}{d_N} - \frac{x_{sh}}{d_N}\right)\right|} \qquad : \bar{\theta}_N > \theta_m \tag{39b}$$

$$\frac{d\left(\frac{V_\perp}{U}\right)_N}{d\left(\frac{cq}{U_\infty}\right)} = \left(\frac{d_N}{c}\right)\left(\frac{\bar{x}_N}{d_N} - \frac{x_{cg}}{d_N} + \frac{\bar{r}_N}{d_N}\tan\bar{\theta}_N\right) \tag{39c}$$

Using the equivalent cone concept for the nosetip, one obtains

$$\frac{\bar{x}_N}{d_N} = -\frac{1}{6}\cot\bar{\theta}N : \frac{\bar{r}_N}{d_N} = \frac{1}{3} \tag{40}$$

A more accurate lumped representation for general nose shapes is

$$\frac{d\left(\frac{V_\perp}{U}\right)_N}{d\left(\frac{cq}{U_\infty}\right)} = \left(\frac{d_N}{c}\right)\frac{(C_{m\alpha})_N}{(C_{N\alpha})_N} \tag{41}$$

The dynamic α derivative, which is generated by convective time lag effects, can be obtained from the variation with time of the induced pressure $\Delta^i Cp$.

$$\Delta^i Cp(t) = \frac{\partial \Delta^i Cp}{\partial(\Delta z/d_N)}\left[\frac{z(x,t)}{d_N} - \frac{z(0,t-\Delta t)}{d_N}\right] + \frac{\partial \Delta^i Cp}{\partial C_{DN}} \frac{\partial C_{DN}}{\partial \alpha}\alpha(0, t - \Delta t) \tag{42}$$

The time increment Δt is defined by Eq. (33). With $z = x\sin\alpha$ (Fig. 1), Eq. (42) becomes

$$\Delta^i Cp(t) = \frac{\partial \Delta^i Cp}{\partial(\Delta z/d_N)}\left[\frac{x - x_{cg}}{d_N}\alpha(t) + \frac{x_{cg}}{d_N}\alpha(t - \Delta t)\right] + \frac{\partial \Delta^i Cp}{\partial C_{DN}} \frac{\partial C_{DN}}{\partial \alpha}\alpha(t - \Delta t) \tag{43}$$

For slow oscillations, $(c\dot{\alpha}/U_\infty)^2 \ll 1$, $\alpha(t-\Delta t)$ is given by the two first terms in a Taylor series, i.e., $\alpha(t-\Delta t)=\alpha(t)-\dot{\alpha}(t)\Delta t$. Thus Eq. (43) can be written

$$\Delta^i Cp(t)=\frac{\partial \Delta^i Cp}{\partial(\Delta z/d_N)}\frac{\mathrm{d}(\Delta z/d_N)}{\mathrm{d}\alpha}\left(\alpha-\frac{x_{cg}}{cg^*}\frac{c\dot{\alpha}}{U_\infty}\right)+\frac{\partial \Delta^i Cp}{\partial C_{DN}}\frac{\partial C_{DN}}{\partial \alpha}\left(\alpha-\frac{x}{cg^*}\frac{c\dot{\alpha}}{U_\infty}\right) \tag{44}$$

The dynamic $\dot{\alpha}$ derivatives defined by Eq. (44) are

$$(\Delta^i Cp\dot{\alpha})_1=-\frac{x_{cg}}{cg^*}(\Delta^i Cp\alpha)_1 \tag{45}$$

$$(\Delta^i Cp\dot{\alpha})_2=-\frac{x}{cg^*}(\Delta^i Cp_\alpha)_2 \tag{46}$$

In the above equations, C_{DN} is the nose drag coefficient referenced to the $\Delta\phi$-sector area $d_N^2\Delta\phi/8$ of the tangent body; that is,

$$C_{DN}=8(C_\gamma Cp_{\max})_{M=M_\infty}\int_{-L_N^*/d_N}^{0}\sin^2(\theta_n+\tau^*)\times\tan\theta_n\frac{r}{d_N}\mathrm{d}\left(\frac{x}{d_N}\right) \tag{47}$$

For a pointed nosetip the flow stagnation point stays at the apex. That is, $L_N^*/d_N=L_N/d_N$ and the angle τ^* is simply the effective angle of attack in the ϕ plane, i.e., $\tau^*=\alpha^*=\sin^{-1}(\sin\alpha\sin\phi)$. However, for a tip with nose roundness, the stagnation point will move away from the body centerline. This reduces the inclination angle with the angle τ_{ST}^* shown in Fig. 3, that is,

$$\begin{aligned}\tau^*&=\alpha^*-\alpha_{ST}^*\\ \alpha^*&=\sin^{-1}(\sin\alpha\sin\phi)\\ \alpha_{ST}^*&=\tan^{-1}\left(\frac{r^*}{d_N}\Big/\frac{L_N^*}{d_N}\right)\end{aligned} \tag{48}$$

The coordinates $y=r^*$ and $x=-L_N^*$ are defined by the vertical tangent at the stagnation point.

$$\begin{aligned}\frac{r^*}{d_N}&=\frac{r}{d_N}\quad\text{for}\quad\theta_n=\frac{\pi}{2}-\alpha^*\\ \frac{L_N^*}{d_N}&=-\frac{x}{d_N}\quad\text{for}\quad\theta_n=\frac{\pi}{2}-\alpha^*\end{aligned} \tag{49}$$

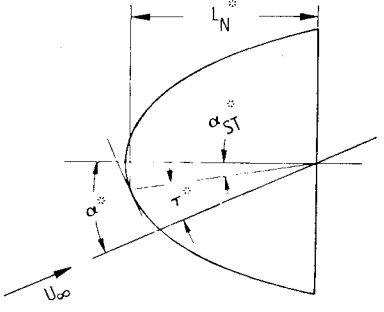

Fig. 3 Effect of angle of attack on nose drag.

In the unsteady case α^* takes the following formulation

$$\begin{aligned}\alpha^*&=\sin^{-1}\left(\frac{V_\perp}{U}\right)_N\\ \left(\frac{V_\perp}{U}\right)_N^*&=\sin\alpha\sin\phi+\left(\frac{d_N}{c}\right)\frac{(C_{m\alpha})_N}{(C_{N\alpha})_N}\sin\phi\frac{cq}{U_\infty}\end{aligned} \tag{50}$$

and one obtains

$$\frac{\partial\tau^*}{\partial\alpha}=\frac{\partial\tau^*}{\partial\left(\frac{V_\perp}{U}\right)_N^*}\frac{\partial\left(\frac{V_\perp}{U}\right)_N^*}{\partial\alpha}=\frac{\partial\tau^*}{\partial\left(\frac{V_\perp}{U}\right)_N}\cos\alpha\sin\phi$$

$$\frac{\partial\tau^*}{\partial\left(\frac{cq}{U_\infty}\right)}=\frac{\partial\tau^*}{\partial\left(\frac{V_\perp}{U}\right)_N}\frac{\partial\left(\frac{V_\perp}{U}\right)_N^*}{\partial\left(\frac{cq}{U_\infty}\right)}=\frac{\partial\tau^*}{\partial\left(\frac{V_\perp}{U}\right)_N^*}\frac{(C_{m\alpha})_N}{(C_{N\alpha})_N}\sin\phi \tag{51}$$

where the derivative $\partial\alpha^*/\partial(V_\perp/U)_N^*$ for the slow oscillations of interest, $(cq/U_\infty)^2\ll 1$, is defined by Eqs. (48) and (50) as follows

$$\frac{\partial\tau^*}{\partial\left(\frac{V_\perp}{U}\right)_N^*}=\frac{\partial\tau^*}{\partial\alpha^*}\frac{\partial\alpha^*}{\partial\left(\frac{V_\perp}{U}\right)_N^*}=\frac{1-\partial\alpha_{ST}/\partial\alpha^*}{\sqrt{1-\sin^2\alpha\sin^2\phi}} \tag{52}$$

Combining Eqs. (47) and (50)-(52) gives

$$C_{DN\alpha}=\frac{\partial C_{DN}}{\partial\left(\frac{V_\perp}{U}\right)_N^*}\cos\alpha\sin\phi \tag{53}$$

$$\frac{\partial C_{DN}}{\partial\left(\frac{cq}{U_\infty}\right)}=\left(\frac{d_N}{c}\right)\frac{\partial C_{DN}}{\partial\left(\frac{V_\perp}{U}\right)_N^*}\frac{(C_{m\alpha})_N}{(C_{N\alpha})_N}\sin\phi \tag{54}$$

$$\frac{\partial C_{DN}}{\partial\left(\frac{V_\perp}{U}\right)_N^*}=8(C_\gamma Cp_{\max})_{M=M_\infty}\int_{-L_N^*/d_N}^{0}\sin 2(\theta_n+\tau^*)\tan\theta_n\frac{1-\partial\alpha_{ST}^*/\partial\alpha^*}{\sqrt{1-\sin^2\alpha\sin^2\phi}}=\frac{r}{d_N}\mathrm{d}\left(\frac{x}{d_N}\right) \tag{55}$$

r/d_N and θ_n are functions of x/d_N, determined by the body geometry.

The aerodynamic characteristics of the embedded body are determined by the following integrations

$$(C_A)_E=\frac{8}{\pi}\left(\frac{d_N}{c}\right)^2\int_{-\phi_1}^{\pi/2}\int_0^{x_B/d_N}Cp_E\tan\theta_\epsilon\frac{r}{d_N}\mathrm{d}\left(\frac{x}{d_N}\right)\mathrm{d}\phi \tag{56}$$

$$(C_{N\alpha})_E=\frac{8}{\pi}\left(\frac{d_N}{c}\right)^2\int_{-\phi_1}^{\pi/2}\int_0^{x_B/d_N}[(Cp_{\alpha L})_1+(Cp_{\alpha L})_2+(\Delta^i Cp_\alpha)_1+(\Delta^i Cp_\alpha)_2]\sin\theta_\epsilon\frac{r}{d_N}\mathrm{d}\left(\frac{x}{d_N}\right)\mathrm{d}\phi \tag{57}$$

$$(C_{m\alpha})_E = -\frac{8}{\pi}\left(\frac{d_N}{c}\right)^3 \int_{-\phi_1}^{\pi/2} \int_0^{x_B/d_N} [(Cp_{\alpha L})_1 + (Cp_{\alpha L})_2 + (\Delta^i Cp_\alpha)_1 + (\Delta^i Cp_\alpha)_2] \left(\frac{x}{d_N} - \frac{x_{cg}}{d_N} + \frac{r}{d_N}\tan\theta_\epsilon\right) \sin\phi \frac{r}{d_N} \mathrm{d}\left(\frac{x}{d_N}\right) \mathrm{d}\phi \tag{58}$$

$$(C_{mq} + C_{m\dot{\alpha}})_E = -\frac{8}{\pi}\left(\frac{d_N}{c}\right)^3 \int_{-\phi_1}^{\pi/2} \int_0^{x_B/d_N} [(Cp_q)_1 + (Cp_q)_2 + (\Delta^i Cp_{\dot{\alpha}})_1 + (\Delta^i Cp_{\dot{\alpha}})_2] \left(\frac{x}{d_N} - \frac{x_{cg}}{d_N} + \frac{r}{d_N}\tan\theta_\epsilon\right) \sin\phi \frac{r}{d_N} \mathrm{d}\left(\frac{x}{d_N}\right) \mathrm{d}\phi \tag{59}$$

The angle ϕ_1 denotes the shadow boundary in the embedded Newtonian flow (as well as in the Newtonian flow on the nose). Only the local shadow boundary is considered. The body shadow cast on a downstream body segment, such as a flare, is ignored as viscous cross flow and entropy wake effects make this downstream shadow concept unrealistic. Thus, ϕ_1 is simply as follows

$$\begin{aligned} \phi_1 &= \pi/2 && : \alpha \le \theta \\ &= \sin^{-1}(\tan\theta/\tan\alpha) && : \alpha > \theta \end{aligned} \tag{60}$$

The nosetip aerodynamics are determined by modified Newtonian theory for the case $\theta_N \le \theta_m$, i.e., when the bow shock is attached.

$$(C_A)_N = \frac{8}{\pi}\left(\frac{d_N}{c}\right)^2 \int_{-\phi}^{\pi/2} \int_{-L_N/d_N}^{0} \times (C_\gamma Cp_{\text{Newt}})_{M=M_\infty} \tan\theta_n \frac{r}{d_N} \mathrm{d}\left(\frac{x}{d_N}\right) \mathrm{d}\phi \tag{61a}$$

$$\times (C_{N\alpha})_N = \frac{8}{\pi}\left(\frac{d_N}{c}\right)^2 \int_{-\phi_1}^{\pi/2} \int_{-L_N/d_N}^{0} \times (C_\gamma Cp_{\alpha_{\text{Newt}}})_{M=M_\infty} \sin\phi_n \frac{r}{d_N} \mathrm{d}\left(\frac{x}{d_N}\right) \mathrm{d}\phi \tag{61b}$$

$$(C_{m\alpha})_N = -\frac{8}{\pi}\left(\frac{d_N}{c}\right)^3 \int_{-\phi_1}^{\pi/2} \int_{-L_N/d_N}^{0} (C_\gamma Cp_{\alpha\text{Newt}})_{M=M_\infty} \times \left(\frac{x}{d_N} - \frac{x_{cg}}{d_N} + \frac{r}{d_N}\tan\theta_n\right) \sin\phi \frac{r}{d_N} \mathrm{d}\left(\frac{x}{d_N}\right) \mathrm{d}\phi \tag{61c}$$

$$(C_{mq})_N = -\frac{8}{\pi}\left(\frac{d_N}{c}\right)^3 \int_{-\phi_1}^{\pi/2} \int_{-L_N/d_N}^{0} (C_\gamma Cp_{q\text{Newt}})_{M=M_\infty} \times \left(\frac{x}{d_N} - \frac{x_{cg}}{d_N} + \frac{r}{d_N}\tan\theta_n\right) \sin\phi \frac{r}{d_N} \mathrm{d}\left(\frac{x}{d_N}\right) \mathrm{d}\phi \tag{61d}$$

Applying Eqs. (61) over the total body length, $-L_N/d_N \le x/d_N \le x_B/d_N$, gives the modified Newtonian characteristics for the complete configuration.

When $L_N/d_N \le 0.5$ and $\theta_N < \theta_m$, the nose aerodynamics are modeled after those valid for the hemisphere nose geometry. Thus, only $(C_A)_N$ is determined by Eqs. (61), and the stability derivatives are obtained as follows

$$\begin{aligned} (C_{N\alpha})_N &= \left(\frac{d_N}{c}\right)^2 (C_{DN})_{\alpha=0} \\ (C_{m\alpha})_N &= \left(\frac{d_N}{c}\right) \frac{x_{cg}}{d_N} (C_{N\alpha})_N \\ (C_{mq})_N &= -\left(\frac{d_N}{c}\right)^2 \left(\frac{x_{cg}}{d_N}\right)^2 (C_{N\alpha})_N \end{aligned} \tag{62}$$

The justification for using Eq. (62) is as follows. It is well known that a significant normal force is generated in the region of the nose-cylinder shoulder, and that this loading increases with the shoulder expansion angle. Using the equivalent cone angle concept, $\bar{\theta}_N$, we find that the shoulder expansion is proportional to $\bar{\theta}_N$, which increases with increasing nose drag. Combining this with the characteristics for a hemisphere nose led to the selection of Eq. (62) as an approximation for the nosetip aerodynamics when $\theta_N < \theta_m$ and $L_N/d_N \le 0.5$.

When better accuracy is needed than what can be provided by Eqs. (61) and (62), one can use the static aerodynamic characteristis, determined numerically or experimentally, to obtain the nosetip contribution to the pitch damping using the following formulation:

$$(C_{mq})_N = -(C_{m\alpha})_N^2 / (C_{N\alpha})_N \tag{63}$$

Discussion of Results

In Fig. 4 present damping predictions are compared with ballistic range data for cylinder-flare bodies with a blunt elliptic nose. It can be seen that the present predictions are in excellent agreement with the experimental results, whereas the Newtonian value greatly overpredicts the damping at hypersonic speeds. It may be somewhat of a surprise that the Newtonian estimate is farther from the experimental results for the larger flare (top of Fig. 4) than for the smaller one (bottom of Fig. 4). The smaller flare is totally submerged in the entropy wake and will, therefore, have a larger reduction

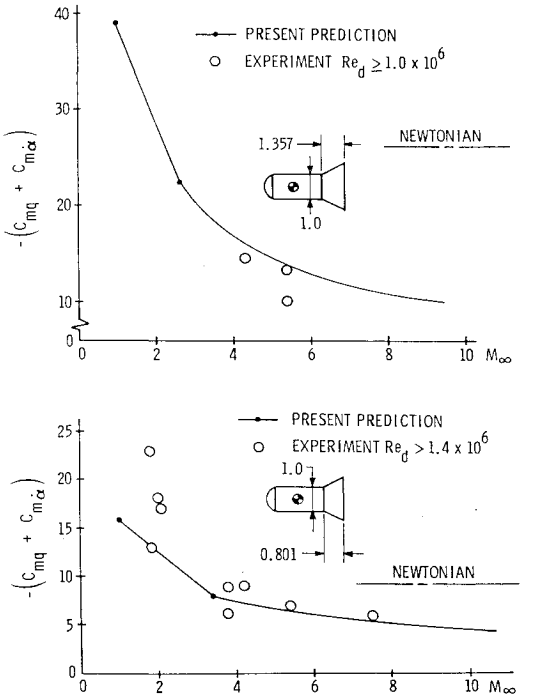

Fig. 4 Predicted and measured damping of blunt-nosed cylinder-flare bodies.

of C_{mq} from the Newtonian value than the larger flare. However, the larger flare has a greater undamping translatory effect, $C_{m\dot{\alpha}}$, because the flare reaches farther out into the entropy wake profile where the velocity gradients are larger.

This entropy gradient effect, $C_{m\dot{\alpha}}$, is neglected in Seiff's theory.[25] The effect of varying the nose bluntness is illustrated in Fig. 5, where present estimates are compared with ballistic range data for a cylinder-flare body with an elliptic nose of varying bluntness.[26] The nose bluntness effect discussed above is not as clearly visible (because of the varying cg location) as the fact that present theoretical predictions are in excellent agreement with experimental results. Figure 6 shows that the present predictions are in equally good agreement with the experimental results for a cylinder-flare body with a slender, blunted ogival nose.

After this succession of excellent agreements between predictions and experiments, the result shown in Fig. 7 for a cylinder-flare body with a blunted conical nose is somewhat of a shock. The experimental results[27] are markedly different from the present inviscid flow prediction. Looking closer at the disagreement between theory and experiment one discovers that the experimental data show less than expected dynamic stability but more than predicted static stability. This opposite effect on static and dynamic stability is a characteristic of flow separation effects.[28-30] Flow investigations[31] show that flow separation indeed occurs on the HB2 model at the Reynolds numbers and hypersonic Mach number of the dynamic test.

At transonic speeds such flare-induced separation jumps to the nose when the angle of attack exceeds a critical value. This is caused by the increasingly adverse pressure gradient as the shock-induced separation moves toward the nose-cylinder shoulder.[32-35] The resulting discontinuous load change causes increased static stability but drastically decreased dynamic stability, leading to overall negative damping.[30] As the adversity of the near-nose pressure distribution decreases fast with increasing supersonic Mach number, it is possible, even likely, that the leeside separated-flow region for the HB2 body increases in a continuous rather than discontinuous fashion with increasing angle of attack. Consequently, the separation-induced decrease of the damping is not large enough to result

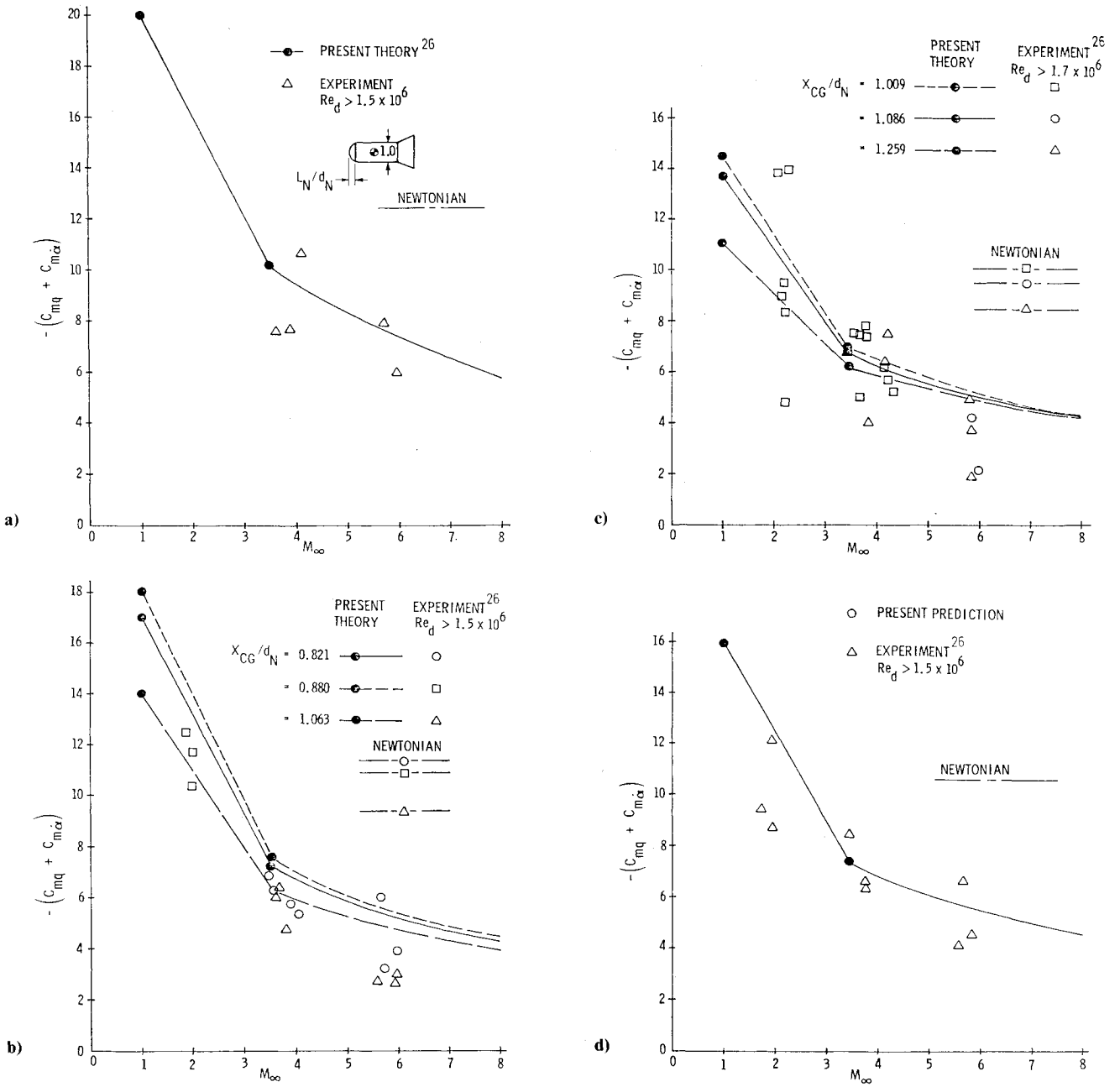

Fig. 5 Predicted and measured damping of flared bodies with elliptic noses of varying bluntness: a) $L_N/d_N = 0.6$; b) $L_N/d_N = 0.4$; c) $L_N/d_N = 0.25$; d) $L_N/d_N = 0.2$.

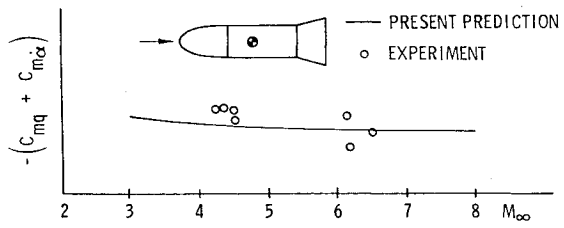

Fig. 6 Predicted and measured damping of a flared body with ogival nose.

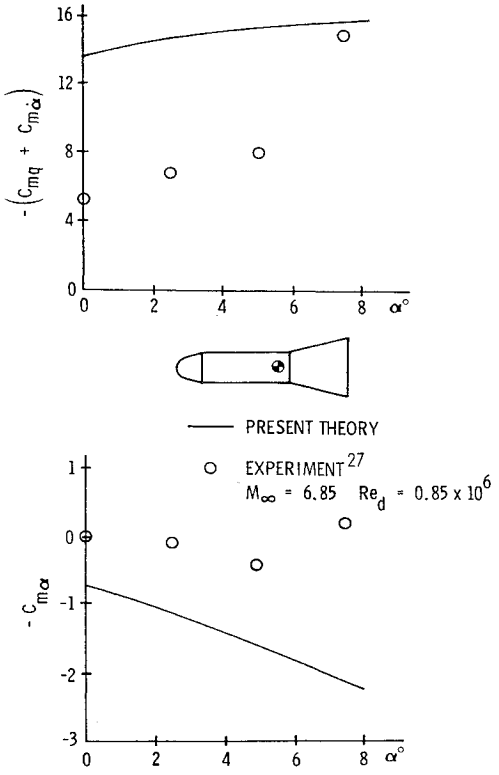

Fig. 7 Effect of angle of attack on the damping of a flared body with a blunted conical nose (HB2 body).

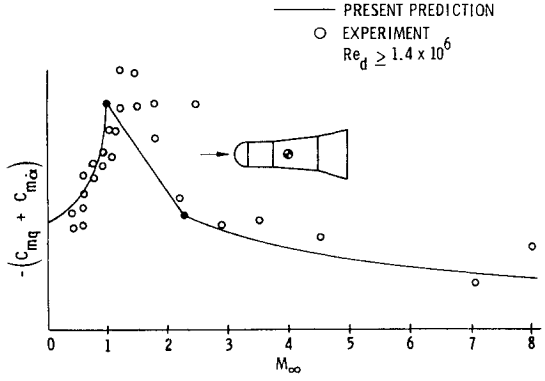

Fig. 8 Predicted and measured damping of a blunt-nosed cylinder body with biconic flare.

in negative damping at hypersonic speeds. However, as Fig. 7 demonstrates, the effect is still large, causing more than a 50% reduction of the damping.

Further support for these Reynolds number effects is provided by the results for hemisphere-nose-bodies with biconic flare¶ (Figs. 8 and 9). Whereas present predictions are

¶As was pointed out earlier, the subsonic data are obtained by the method of Ref. 2. A straight-line fairing is used between $M_\infty = \bar{M}^*_\infty$ and $M_\infty = 1$.

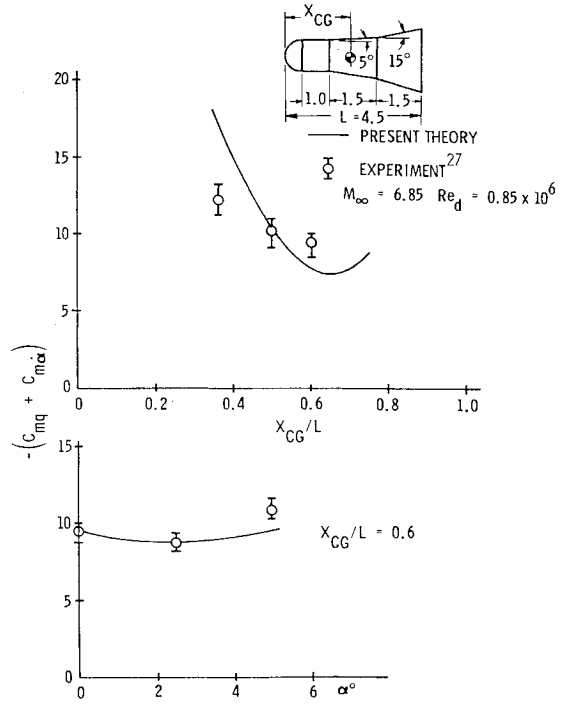

Fig. 9 Effect of oscillation center on the damping of a hemisphere-cylinder body with biconic flare.

in excellent agreement with the experimental results obtained at high Reynolds numbers (Fig. 8), the agreement with low Reynolds number data is not quite as good[27] (Fig. 9). However, it is better than for the simple flare[27] (Fig. 7), probably because the milder adverse pressure gradient supplied by the biconic flare causes less flow separation than the simple flare.

Conclusions

As far as the author knows the presented analysis is the only one capable of predicting the dynamic characteristics for the type of missile geometries discussed in this paper. The comparison with experimental results demonstrates that the developed fast computational method has the accuracy needed for preliminary design.

Acknowledgment

This paper is based upon results obtained in studies performed under Contracts N62269-73C-0713 and N60921-77C-A294 for NADC, Warminster, Penn., and NSWC, Dahlgren, Va., respectively.

References

[1] Ericsson, L.E., "Unsteady Aerodynamics of an Ablating Flared Body of Revolution Including Effects of Entropy Gradient," *AIAA Journal*, Vol. 6, Dec. 1968, pp. 2395-2401.

[2] Ericsson, L.E., "Effect of Mach Number on Slender Vehicle Dynamics," *Journal of Spacecraft and Rockets*, Vol. 19, Jan.-Feb. 1981, pp. 18-23.

[3] Ericsson, L.E., "Generalized Unsteady Embedded Newtonian Flow," *Journal of Spacecraft and Rockets*, Vol. 12, Dec. 1975, pp. 718-726.

[4] Ericsson, L.E. and Guenther, R.A., "Effect on Slender Vehicle Dynamics of Change from Spherical to Conical Nose Bluntness," *Journal of Spacecraft and Rockets*, Vol. 9, June 1972, pp. 435-440.

[5] Ericsson, L.E. and Guenther, R.A., "Prediction of Nonlinear Stability Characteristics of Slender Cones with Conical Nose Bluntness," *AIAA Journal*, Vol. 10, Aug. 1972, pp. 1111-1113.

[6] Seiff, A. and Whiting, E.E., "Calculation of Flow Fields from Bow-Wave Profiles for the Downstream Region of Blunt-Nosed Circular Cylinders in Axial Hypersonic Flight," NASA TND-1147, Nov. 1961.

[7] Seiff, A., "Secondary Flow-Fields Embedded in Hypersonic Shock Layers," NASA TND-1304, May 1962.

[8] Gravalos, F.G., Edfelt, I.H., and Emmons, H.W., "The Supersonic Flow About a Body of Revolution for Gases at Chemical Equilibrium" *Proceedings of the IX International ASTR Congress,* Amsterdam, Aug. 1958, pp. 312-332.

[9] Seiff, A. and Whiting, E.E., "A Correlation Study of the Bow-Wave Profiles of Blunt Bodies," NASA TND-1148, Feb. 1962.

[10] Katz, J.R., "Pressure and Wave Drag Coefficients for Hemispheres, Hemisphere-Cones, and Hemisphere-Ogives," Rept. 5849, Naval Ordnance Research Lab., March 21, 1958.

[11] Lukasiewicz, J., "Hypersonic Flow-Blast Analogy," AEDC-TR-61-4, June 1961.

[12] Van Hise, V., "Analytic Study of Induced Pressure on Long Bodies of Revolution with Varying Nose Bluntness at Hypersonic Speeds," NASA-TR-R-78, 1960.

[13] Swigart, R.J., "On the Shock Shape and Pressure Distribution about Blunt-Nosed Cylinders Using Blast Wave Theory," *Journal of Aeronautical Science,* Vol. 28, Oct. 1961, pp. 828-829.

[14] Sinnot, C.S., "An Analysis of Shock Detachment Distance in Supersonic Flow," ARC 21,078, Aeronautical Research Council, Great Britain, 1958.

[15] Stollery, J.L. and Maull, D.J., "A Note on Shock Detachment Distance," *Journal of the Royal Aeronautical Society,* Vol. 64, June 1960, pp. 357-359.

[16] Shanbag, V.V., "An Empirical Expression for Maximum Cone Angle for Attached Shock at Supersonic Mach Numbers," *Journal of Aircraft,* Vol. 7, March-April 1970, p. 191.

[17] Ames Research Staff, "Equations, Tables, and Charts for Compressible Flow," NACA Report 1135, 1953.

[18] Holt, C.P., "On the Inviscid Tail Efficiencies of Slender Configurations at Hypersonic Speeds," *Journal of Aeronautical Science,* Vol. 29, June 1962, p. 748.

[19] Lin, S.C., "Cylindrical Shock Waves Produced by Instantaneous Energy Release," *Journal of Applied Physics,* Vol. 25, Jan. 1954, pp. 54-57.

[20] Kuehn, D.M., "Experimental and Theoretical Pressures on Blunt Cylinders for Equilibrium and Nonequilibrium Air at Hypersonic Speeds," NASA TND-1979, 1963.

[21] Eaves, R.N. Jr., "An Empirical Correlation of Pressure on Blunt-Nosed Cylindrical Afterbodies at Hypersonic Mach Numbers," AEDC-TR-68-82, May 1968.

[22] Ericsson, L.E. and Reding, J.P., "Dynamic Stability Problems Associated with Flare Stabilizers and Flap Controls," *Journal of Spacecraft and Rockets,* Vol. 7, Feb. 1970, pp. 132-137.

[23] Ericsson, L.E., "Unsteady Embedded Newtonian Flow," *Astronautica Acta,* Vol. 18, Nov. 1973, pp. 309-330.

[24] Ericsson, L.E. and Reding, J.P., "Approximate Slender Vehicle Dynamics at All Speeds," *Proceedings of 11th Navy Symposium on Aeroballistics,* Aug. 1978, Vol. 1, pp. 87-114.

[25] Seiff, A. and Whiting, E.E., "The Effects of the Bow Shock Wave on the Stability of Blunt Nosed Slender Bodies," NASA TMX-377, Sept. 1960.

[26] Levensteins, Z.J., "Ballistic Range Firings for Determination of Drag and Stability of Models of Five Polaris Configurations," NOLTR 61-35, Aug. 1961.

[27] East, R.A., Quasrawi, A.M.S., and Khalid, M., "An Experimental Study of the Hypersonic Dynamic Stability of Pitching Blunt Conical and Hyperballistic Shapes in a Short Running Time Facility," *AGARD Conference on Dynamic Stability Parameters,* AGARD-CP-235, Athens, Greece, May, 1978.

[28] Ericsson, L.E. and Reding, J.P., "Aerodynamic Effects of Bulbous Bases," NASA CR-1339, Aug. 1969.

[29] Ericsson, L.E., "Unsteady Aerodynamics of Separating and Reattaching Flow on Bodies of Revolution," *Recent Research on Unsteady Boundary Layers,* Vol. 1, IUTAM Symposium Laval University, Quebec, May 1971, pp. 481-512.

[30] Ericsson, L.E., "Separated Flow Effects on Static and Dynamic Stability of Blunt-Nosed Cylinder Flare Bodies," NASA CR-76919, Dec. 1965.

[31] Gray, J.D. and Lindsay, E.E., "Force Tests of Standard Hypervelocity Ballistic Models HB-1 and HB-2 at Mach 1.5 to 10," AEDC-TDR-63-137, Aug. 1963.

[32] Ericsson, L.E., "Loads Induced by Terminal-Shock Boundary-Layer Interaction on Cone-Cylinder Bodies," *Journal of Spacecraft and Rockets,* Vol. 7, Sept. 1970, pp. 1106-1112.

[33] Ericsson, L.E., "Aeroelastic Instability Caused by Slender Payloads," *Journal of Spacecraft and Rockets,* Vol. 4, Jan. 1967, pp. 65-73.

[34] Robertson, J.E. and Chevalier, H.L., "Characteristics of Steady-State Pressures on the Cylindrical Portion of Cone-Cylinder Bodies at Transonic Speeds," AEDC-TDR-63-104, Aug. 1963.

[35] Chevalier, H.L. and Robertson, J.E., "Pressure Fluctuations Resulting from Alternating Flow Separation and Attachment at Transonic Speeds," AEDC-TDR-63-204, Nov. 1963.